Nonadiabaticity of cavity-free neutral nitrogen lasing

Pengji Ding,[1,2] Juan Carlos Escudero,[3] Aurélien Houard,[1] Alberto Sanchis,[3] Javier Vera,[3] Sergio Vicéns,[3] Yi Liu,[1,4,*] and Eduardo Oliva[3,5,†]

[1]*Laboratoire d'Optique Appliquée, ENSTA ParisTech, CNRS, Ecole Polytechnique, Université Paris-Saclay, F-91762 Palaiseau Cedex, France*

[2]*Division of Combustion Physics, Department of Physics, Lund University, P.O. Box 118, SE-221 00 Lund, Sweden*

[3]*Departamento de Ingeniería Energética, ETSI Industriales, Universidad Politécnica de Madrid, E-28006 Madrid, Spain*

[4]*Shanghai Key Lab of Modern Optical System, University of Shanghai for Science and Technology, Shanghai 200093, China*

[5]*Instituto de Fusión Nuclear, Universidad Politécnica de Madrid, E-28006 Madrid, Spain*

(Received 22 May 2017; published 7 September 2017)

We report on a theoretical study of cavity-free lasing of neutral nitrogen molecules in femtosecond laser filaments with a nonadiabatic Maxwell-Bloch model, compared with recent pump-seed experiments. The nonadiabaticity of the lasing process is revealed and it is found that electron-neutral collisions dominate the dipole dephasing rate. Moreover, we show that the asymmetry between forward and backward lasing not only depends on the different amplification lengths but also on the temporal dynamics of electron-neutral collisions. The comparison of the nonadiabatic model with simulations based on the adiabatic approximation (such as radiative transfer equations) explicitly sets a bound on the validity of the latter model for cavity-free nitrogen lasing phenomenon, which holds a unique potential in optical remote sensing applications.

DOI: 10.1103/PhysRevA.96.033810

I. INTRODUCTION

The interest in coherent emission from atmospheric constituents pumped by ultrafast lasers has been rising in recent years, mainly because of its huge potential in remote sensing applications [1–9]. While nowadays remote sensing techniques rely on detecting backward-scattered light from targets in the atmosphere, backward lasing from a certain point in the sky towards ground-based detectors is expected to improve tremendously the efficiency and precision of these techniques [10]. It has been recently demonstrated that intense, circularly polarized, infrared pulses ($\lambda = 800$ nm) can create a filamentary plasma in air that amplifies the spontaneous emission of neutral nitrogen molecules ($\lambda = 337.1$ nm) in the backward direction [11]. Forward (i.e., propagating with the IR pulse) and backward (i.e., counterpropagating with the IR pulse) amplified emissions of both injected UV and spontaneous emission have been achieved in pure nitrogen [9,11–14] or mixed with argon [6]. In air, only forward amplified emission has been observed [12,13]. The absence of backward amplification in air is explained by the pronounced asymmetry of the lasing intensity between backward and forward geometries in favor of the latter and the quenching effect of oxygen molecules [11,13]. Thus, it is of capital importance to study the origin of this asymmetry in order to envision strategies allowing backward lasing in air.

Plasma amplifiers can be probed with the use of an UV, XUV, or soft x-ray seed pulse tuned to the lasing wavelength. The comparison of experimental results with proper modeling allows one to benchmark the codes and to quantify parameters such as collisional rates, populations, electron density, etc., that are very difficult to measure experimentally. For example, the gain lifetime and the gain recovery time of plasma-based soft x-ray lasers were successfully measured using amplified spontaneous emission (ASE) [15] and high-order harmonics [16] as seed pulses. This pump-seed technique has been widely used to study the superradiance of excited N_2^+ molecules [17], the dependence of the optical gain in N_2^+ molecules with pressure [18], and the local gain coefficient of excited nitrogen molecules in air [19]. Amplification curves of N_2 and N_2^+, pure, mixed with Ar, and in air were measured in Refs. [12,13,20,21]. More recently, amplification curves along with the temporal profile of forward and backward lasing from neutral nitrogen molecules at $\lambda = 337.1$ nm, for both amplified seed and amplified spontaneous emission, were measured [9].

Different models are available to study the amplification of UV radiation in filaments. Radiative-transfer-based models have been used to study pure molecular nitrogen emission [14] or in air [3,7,22]. Maxwell-Bloch models have been used to study the emission of atomic oxygen in air [4], superluminescence and superradiance of atmospheric contaminants [1], and the emission and amplification in pure molecular nitrogen filaments [9]. The accuracy of these models depends on the approximations needed to deduce them, among other factors. For example, the use of a radiative transfer equation assumes implicitly the adiabatic approximation for the polarization and a constant dipole dephasing rate, as it will be explained. Several Maxwell-Bloch models also neglect the temporal dynamics of the dipole dephasing rate and most of them assume a Maxwellian electron energy distribution function. Some improvements over these approximations are reported in Refs. [14,22], where the electron energy distribution function is computed explicitly, and in Ref. [9], where we use our fully time-dependent, one-dimensional, nonadiabatic Maxwell-Bloch code DEEPONE [16,23].

In this paper, we analyze the range of validity of the adiabatic approximation, widely used to model cavity-free nitrogen lasing. In Sec. II, we describe our plasma and Maxwell-Bloch models. Since the collisional dephasing rate plays a fundamental role in the temporal dynamics of the amplification and, thus, on the validity of the adiabatic approximation, we dedicate Sec. III to the study of this

*yi.liu@usst.edu.cn
†eduardo.oliva@upm.es

rate. We will show that a constant dephasing rate (as the one induced by neutral-neutral collisions) cannot explain the experimental results. We will thus conclude that the dephasing rate is dominated by electron-neutral collisions, inducing a decreasing dipole dephasing rate that explains the different amplifications and durations of forward and backward emission. In Sec. IV, we will show with both a toy model for the polarization density and full Maxwell-Bloch simulations that the adiabatic approximation cannot reproduce the temporal dynamics of amplification, finding a dramatic divergence with experimental results in the case of backward amplification. Nevertheless, our study reveals that the adiabatic approximation performs quite well when modeling quantities integrated in time, such as the total emitted energy. Finally, we will conclude in Sec. V with a brief summary of the article, the enumeration of other laser systems where the conclusions of this paper hold, and future improvements of the present model.

II. MAXWELL-BLOCH MODELLING

Our one-dimensional, time-dependent, nonadiabatic Maxwell-Bloch code DEEPONE [16,23] solves the paraxial wave equation for the electric field in the slowly varying envelope approximation

$$\frac{\partial E_\pm}{\partial t} \pm c\frac{\partial E_\pm}{\partial z} = \frac{i\omega_0}{2}\left[\frac{P_\pm}{\epsilon_0} - \left(\frac{\omega_p}{\omega_0}\right)^2 E_\pm\right], \tag{1}$$

where E_+, E_- are respectively the forward and backward propagating electric fields, P_+, P_- the corresponding polarization densities, c is the light velocity in vacuum, ω_0 is the frequency of the electric field, ω_p is the free-electron plasma frequency, and ϵ_0 is the vacuum permittivity. The polarization density is computed using a constitutive relation derived from Bloch equations,

$$\frac{\partial P_\pm}{\partial t} = \Gamma - \gamma P_\pm - \frac{i z_{ul}^2}{\hbar} E_\pm (N_u - N_l), \tag{2}$$

where Γ is a stochastic source term with a vanishing correlation time that takes into account the spontaneous emission [24,25], γ is the dipole dephasing rate due to collisions, z_{ul} is the nondiagonal dipole matrix element which is obtained from Einstein's A_{ul} coefficient, $z_{ul} = \sqrt{3\pi A_{ul}\hbar c^3 \epsilon_0 \omega_0^{-3}}$, and N_u, N_l are respectively the population of the upper and lower levels of the lasing transition (levels $C\,^3\Pi_u^+$ and $B\,^3\Pi_g^+$ in the triplet manifold of the neutral nitrogen molecule). The populations of the levels are computed using rate equations,

$$\frac{\partial N_i}{\partial t} = \sum_k C_{ki} N_k \pm \mathrm{Im}(E^* P)\frac{1}{2\hbar}, \tag{3}$$

where the summation is extended to all levels taken into account, three in our case ($X\,^1\Sigma_g$, $B\,^3\Pi_g^+$, $C\,^3\Pi_u^+$); $i = u, l$ and C_{ki} are the collisional (de)excitation and radiative deexcitation rates. These rates are computed using the cross sections reported in Ref. [26]. The product of the cross section and velocity is integrated using the energy distribution function of the free electrons. In our computations, we have assumed a Maxwell distribution corresponding to the temperature computed as stated below. However, in Ref. [14] it is reported that the electron energy distribution function departs from a Maxwellian distribution function during several tens of picoseconds, resulting in an enhanced pumping of the lower level of the transition during the first 20–25 ps. Thus, this departure from equilibrium strongly reduces the population inversion. In order to take into account this effect, we have artificially enhanced the lower level pumping rate by flooring the corresponding collisional rate during the first 20 ps of the simulation. The resulting population inversion is in good agreement with that reported in Ref. [14]. More importantly, our model reproduces quite well the experimental amplification curve [9] which is directly related to the population inversion when the laser is not saturated, as it is the case in this work.

Due to the employment of the slowly varying envelope approximation, we are treating the field envelope, not the laser field. As a result, the beating effect observed experimentally [9] cannot directly appear in our Maxwell-Bloch simulations. Thus, we postprocessed our electric field data assuming an interference effect between sublevels. When the arbitrary phases between the three fields are correct, the positions of the experimental maxima and minima are retrieved.

The evolutions of the electron density and temperature of the plasma are computed following the lines described in Refs. [3,7,9]. The electron temperature T_e and the vibrational temperature T_v are computed from the following equations,

$$\frac{3}{2}\frac{\partial N_e T_e}{\partial t} = -Q_c N_a N_e\left(1 - \frac{T_v}{T_e}\right),$$
$$\frac{3}{2}N_a\frac{\partial T_v}{\partial t} = Q_c N_a N_e\left(1 - \frac{T_v}{T_e}\right),$$

where N_e and N_a are respectively the electron and neutral density, and Q_c is the cooling rate, given by

$$Q_c \approx 3.5\times 10^{-8}\exp\left(-\frac{5}{3T_e}\right) + 6.2\times 10^{-11}\exp\left(-\frac{1}{3T_e}\right),$$

valid for $T_e < 2$ eV. For higher temperatures the value of Q_c is extrapolated. The fast cooling of the filament (the initial temperature of 16 eV [27] cools in less than 6 ps to a value lower than 2 eV) ensures that extrapolation errors are low enough to not affect the simulation.

The electron, positive, and negative ion densities N_e, N_p, and N_n are given by

$$\frac{\partial N_e}{\partial t} = \nu_{\mathrm{ion}} N_e - \beta N_p N_e - \eta N_e,$$
$$\frac{\partial N_n}{\partial t} = \eta N_e - \beta_{np} N_n N_p,$$
$$N_p = N_e + N_n,$$

where ν_{ion} is the collisional ionization rate, β is the electron-ion recombination rate, β_{np} is the ion recombination rate, and η the attachment coefficient. In Ref. [3] the following analytical expressions are given for those coefficients:

$$\nu_{\mathrm{ion}} = \nu_{\mathrm{N_2}}\left(\frac{T_e}{U_{\mathrm{N_2}}}\right)^{3/2}\left(\frac{U_{\mathrm{N_2}}}{T_e} + 2\right)\exp\left(-\frac{U_{\mathrm{N_2}}}{T_e}\right),$$
$$U_{\mathrm{N_2}} = 15.6\ \mathrm{eV}, \quad \nu_{\mathrm{N_2}} = 7.6\times 10^{11}\ \mathrm{s}^{-1},$$
$$\beta(\mathrm{cm}^3/\mathrm{s}) \approx 1.5\times 10^{-8} T_e^{-0.7}, \quad \text{for } T_e < 0.1\ \mathrm{eV},$$

$$\beta(\mathrm{cm}^3/\mathrm{s}) \approx 2.0 \times 10^{-8} T_e^{-0.56}, \quad \text{for } T_e > 0.1 \text{ eV},$$
$$\eta(\mathrm{s}^{-1}) = \alpha_2 N_a + \alpha_3 N_a^2,$$
$$\alpha_2(\mathrm{cm}^3/\mathrm{s}) \approx 2.75 \times 10^{-10} T_e^{-0.5} \exp\left(-\frac{5}{T_e}\right),$$
$$\alpha_3(\mathrm{cm}^3/\mathrm{s}) \approx 1.5 \times 10^{-32} T_e^{-1} \exp\left(-\frac{0.052}{T_e}\right).$$

It is important to mention that the above expressions were reported in studies of nitrogen lasing in air (i.e., mixed with oxygen). However, the agreement between modeling and experimental results [9] allows us to conclude the validity of the model for pure nitrogen lasing.

III. MODELIZATION OF THE COLLLISIONAL DEPHASING RATE

The collisional dipole dephasing rate γ is a key parameter that controls the temporal dynamics of the amplification of UV radiation. Depending on the physical mechanism that causes the dephasing, this rate will take greater or lower values and, more importantly, it will evolve in time differently. For example, in plasma-based soft x-ray lasers the radiation is amplified by ions. Thus, the dipole dephasing rate is taken as the electron-ion collision frequency [24] $\gamma \propto N_e T_e^{-\frac{3}{2}}$. Previous works on atmospheric lasing assume explicitly a constant dipole dephasing rate [1,4,14,22], or implicitly using a constant stimulated emission cross section [3,7] [which implies assuming a Lorentzian line shape of constant width $\Delta\omega$ and thus a constant collisional rate; see Eq. (6)]. When the depolarization is dominated by collisions with neutral molecules, the collision rate can be approximated by a constant value, since it takes the form [28] $\gamma \approx \langle \sigma v_n \rangle N_n$. All three parameters, the neutral density N_n, the cross section σ, and the velocity $v \propto T_n^{\frac{1}{2}}$, are almost constant during the emission time, since the temperature of the neutrals T_n varies in a slower time scale. However, a constant dipole dephasing rate cannot explain the huge difference between the temporal profile and amplification of the forward and backward amplified pulses. As shown in Fig. 1(a), the forward seeded emission can be modeled using a constant value for the dipole dephasing rate, $\gamma = 8.3 \times 10^{11}$ s^{-1} [14,29]. Since the delay between the IR pulse and the UV emission is fixed in the forward regime, we can assume that the UV pulse will find the same plasma conditions all along the amplifier. However, the temporal profile of the ASE and backward seeded emission, depicted in Figs. 1(a) and 1(b), differ from the experimental one, as shown in Figs. 1(e) and 1(f). Using a lower value for the dipole dephasing rate, $\gamma = 10^{11}$ s^{-1}, widens the backward amplified pulse (although its duration is still shorter than the experimentally measured) and strongly overestimates the intensity of forward pulses, as represented in Figs. 1(c) and 1(d).

These negative results can be explained as follows. Experimentally, the ASE emission, spanning 30–40 ps, interacts with a decreasing profile of the dipole dephasing rate, strongly increasing the cross section, since it is inversely proportional to the dipole dephasing rate [as shown later in Eq. (6)]. When the dipole dephasing rate is taken as a constant, the cross

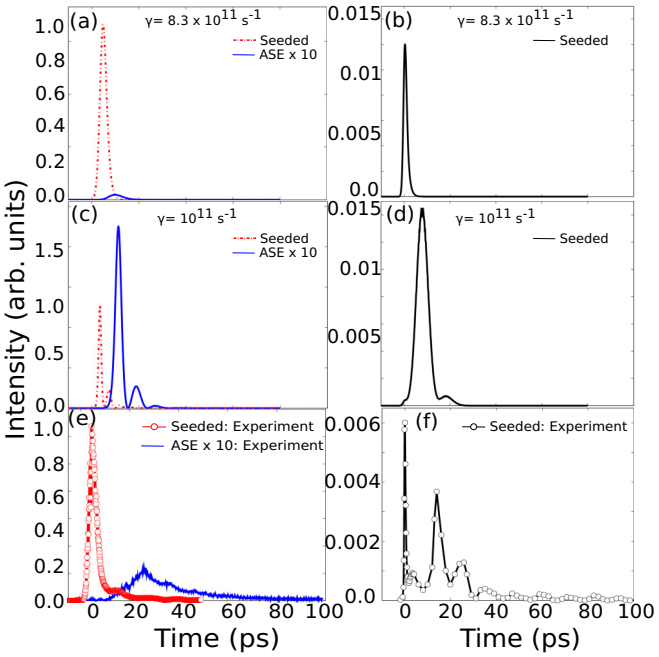

FIG. 1. (a), (c) Forward and (b), (d) backward amplified seed (red dotted line/black continuous line) and ASE (blue continuous line) modeled using constant values for the dipole dephasing rate, $\gamma = 8.3 \times 10^{11}$ s^{-1} (upper panel) and $\gamma = 10^{11}$ s^{-1} (lower panel). Comparison with experiments [9] (e), (f) shows that a constant dipole dephasing rate cannot explain the experimental results.

section and thus the amplification of ASE is too low, as shown in Fig. 1(a) for $\gamma = 8.3 \times 10^{11}$ s^{-1}, or too high, as shown in Fig. 1(c) for $\gamma = 10^{11}$ s^{-1}. The backward regime is more complex. Due to its counterpropagating nature, the amplified UV pulse will sweep all the temporal dynamics of the plasma from the moment when it encounters the IR pulse at half the length of the amplifier. In conclusion, a constant dipole dephasing rate cannot explain the experimental results. These differences in the temporal profile are a clear signature of a strong variation of the dipole dephasing rate, diminishing with time and thus increasing the duration of the pulse.

This decrease on the collisional dipole dephasing rate can be explained if we assume that this rate is dominated mainly by electron-neutral collisions, taking the form $\gamma = \langle \sigma v \rangle N_e \propto N_e T_e^{\frac{1}{2}}$. Figure 2 shows the temporal dynamics of the electron-neutral collision dipole dephasing rate. This rate has been computed using cross sections obtained from Ref. [26] and assuming a Maxwellian electron energy distribution function. The absolute value of the dephasing rate is normalized to a value of $\gamma_0 = 8.3 \times 10^{11}$ s^{-1} at $t = 4$–5 ps, as reported experimentally [9,14,29]. The fast cooling of free electrons [9,14,22] along with the diminishing electron density, due to recombination, explains the one order of magnitude variation of the collisional dipole dephasing rate, from $\gamma \approx 10^{12}$ s^{-1} at the very first moments to $\gamma < 1.5 \times 10^{11}$ s^{-1} after 100 ps.

Figure 3 shows good agreement between experiment and our model when using the time-dependent dipole dephasing rate of Fig. 2. However, our model gives higher intensities for ASE (two times higher) and the backward amplified seed (five times higher). In addition to this, the backward

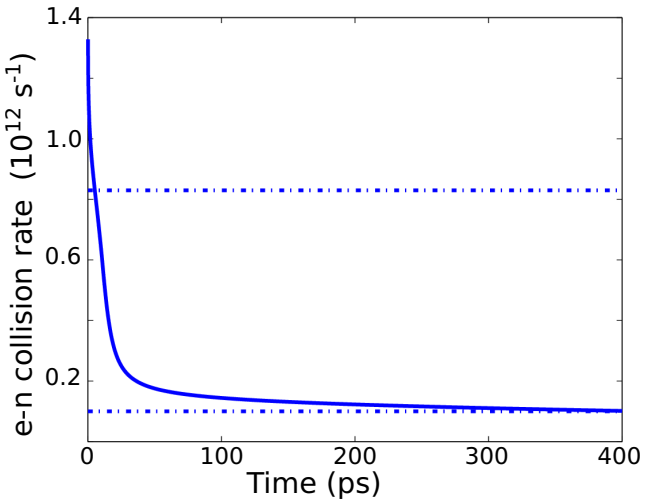

FIG. 2. Temporal evolution of the dipole dephasing rate induced by electron-neutral collisions (solid blue line). The two constant dipole dephasing rates used in Fig. 1 are depicted (dashed-dotted blue line) for comparison.

amplified seed seems longer in the experiment. The fact that we used a Maxwellian electron energy distribution function to compute γ could explain this slight mismatch. In addition to this, plasma hydrodynamics may play a role in backward amplification, further reducing the electron density. This reduction implies a lower γ and thus a longer pulse. In spite of this, our Maxwell-Bloch model, enhanced with a time-dependent dipole dephasing rate, explains the asymmetry between forward and backward lasing quite well.

It is worth mentioning that the need for time-dependent dipole dephasing rates is directly applicable to schemes that rely on the emission of excited molecular nitrogen ions [17,18,20,30,31]. In these schemes, electron-ion collisions

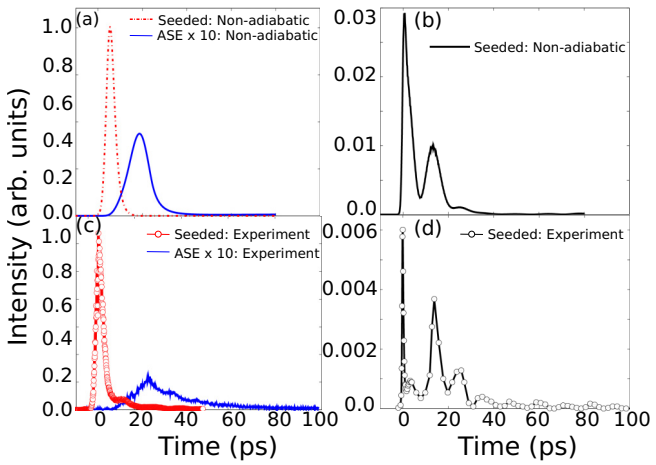

FIG. 3. (a) Forward and (b) backward amplified seed (red dotted line/black continuous line) and ASE (blue continuous line) modeled using a time-dependent dipole dephasing rate, induced by electron-neutral collisions (depicted in Fig. 2). The experimental results [9] for (c) forward and (d) backward emission of neutral molecular nitrogen are shown below.

will dominate the dipole dephasing rate, taking the form $\gamma \propto N_e T_e^{-\frac{3}{2}}$. Thus, the dipole dephasing rate will vary inversely and faster with the electron temperature than the case of neutral molecular nitrogen.

IV. ADIABATIC VERSUS TIME-DEPENDENT MODEL

The set of equations (1)–(3) can be simplified using the so-called adiabatic approximation. In this approximation we assume that the medium perturbed by the electric field reacts immediately. In this way, the polarization density is proportional to the electric field and it can be written as $P = \epsilon_0 \chi E$, where χ is the electric susceptibility. The steady-state solution of Eqs. (2) and (3), neglecting the spontaneous emission contribution, allows one to find an expression for the imaginary part of the susceptibility $\chi = \chi' - i\chi''$ [32],

$$\chi'' = \frac{z_{ul}^2}{\hbar \gamma \epsilon_0}(N_u - N_l). \tag{4}$$

Within the adiabatic approximation, a radiative transfer equation can be deduced, obtaining the following equation,

$$\frac{\partial I}{\partial z} = \sigma_{\text{stim}}(N_u - N_l)I - \Gamma_d I, \tag{5}$$

where Γ_d is a damping term depending on the ratio ω_p/ω_0. The stimulated emission cross section (assuming a Lorentzian line shape) $\sigma_{\text{stim}}(\omega_0)$ is given by

$$\sigma_{\text{stim}}(\omega_0) = \frac{\omega_0 z_{ul}^2}{2\hbar\epsilon_0 c}\frac{4}{\Delta\omega} = \frac{\omega_0 z_{ul}^2}{\hbar\gamma\epsilon_0 c}, \tag{6}$$

where the full width at half maximum (FWHM) of the Lorentzian line shape is $\Delta\omega = 2\gamma$, deduced within the Maxwell-Bloch formalism [24,33].

The validity of this approximation, extensively used to model nitrogen lasing [3,7,14,22], and thus its predictive capacity, must be examined in order to model cavity-free nitrogen lasers. A straightforward way would be by comparing its results with pump-seed experiments. However, before this comparison is done, deducing an estimation of the range of validity of the adiabatic approximation or, conversely, the radiative transfer equation, will prove useful to understand the role of the temporal dynamics of the plasma in the amplification of UV radiation. This estimation can be done as follows.

An exact solution for Eq. (2) can be obtained provided some assumptions are made. When the polarization is excited by an external electric field (i.e., an UV seed pulse), the spontaneous emission term can be neglected. Assuming that the electric field is switched on at $t = 0$, and that both the dipole dephasing rate and the population inversion remain constant all along the pulse duration (i.e., far from the saturation regime), the solution of Eq. (2) is

$$P_{\text{NA}}(t) = -\frac{i z_{ul}^2}{\hbar}(N_u - N_l)e^{-\gamma t}\int_0^t E(\tau)e^{\gamma\tau}d\tau. \tag{7}$$

The above-mentioned assumptions are valid at the entrance of the plasma and for seed pulses of several picoseconds of duration or shorter, as the ones used in the experiments studied here.

Assuming that the intensity of the seed pulse has a Gaussian temporal shape, the electric field takes the form $E(t) = E_0 e^{-\frac{(t-t_{\rm cent})^2}{2\sigma^2}}$, where $t_{\rm cent}$ is the time when the maximum of the pulse arrives and σ is its standard deviation.

After some algebra, we can write Eq. (7) as

$$P_{\rm NA}(t) = -\frac{iz_{ul}^2}{\hbar}(N_u - N_l)E_0 e^{\frac{\gamma^2\sigma^2}{2}} e^{-\gamma(t-t_{\rm cent})}\sqrt{2\pi}\sigma \times [F(t;t_{\rm cent}+\gamma\sigma^2,\sigma) - F(0;t_{\rm cent}+\gamma\sigma^2,\sigma)], \tag{8}$$

where $F(t;\tau,\sigma)$ is the distribution function of a Gaussian probability density function centered at τ and with standard deviation σ.

The adiabatic polarization for the same UV seed pulse takes the form

$$P_{\rm ad}(t) = -\frac{iz_{ul}^2}{\hbar}(N_u - N_l)\frac{E_0}{\gamma}e^{-\frac{(t-t_{\rm cent})^2}{2\sigma^2}}. \tag{9}$$

The maximum values can be compared immediately. The adiabatic polarization attains its maximum value $P_{\rm ad}(t_{\rm max}^{\rm ad}) = -\frac{iz_{ul}^2}{\hbar}(N_u - N_l)\frac{E_0}{\gamma}$ at $t_{\rm max}^{\rm ad} = t_{\rm cent}$. For the time-dependent polarization, it can be shown that at its maximum

$$F\left(t_{\rm max}^{\rm NA};\tau,\sigma\right) - F(0;\tau,\sigma) = \frac{1}{\sqrt{2\pi}\sigma\gamma}e^{-\frac{(t_{\rm max}^{\rm NA}-\tau)^2}{2\sigma^2}}, \tag{10}$$

with $\tau = t_{\rm cent} + \gamma\sigma^2$.

After some algebra we obtain a relation between the maximum value of the nonadiabatic and adiabatic polarization,

$$\frac{P_{\rm NA}\left(t_{\rm max}^{\rm NA}\right)}{P_{\rm ad}\left(t_{\rm max}^{\rm ad}\right)} = e^{-\frac{(t_{\rm max}^{\rm NA}-t_{\rm max}^{\rm ad})^2}{2\sigma^2}}. \tag{11}$$

Thus, the adiabatic approximation systematically overestimates the maximum value of the polarization. While there is no algebraic formula for $t_{\rm max}^{\rm NA}$ [it is computed from Eq. (10)] it is worth noting that it depends on the duration of the seed pulse, via σ, and the dipole dephasing rate γ. The greater the dipole dephasing rate, the better is the adiabatic approximation. Indeed, γ is the inverse of the characteristic time of the plasma response to a probe electric field [23]. When this time is significantly shorter than the pulse duration, the polarization evolves fast enough to accommodate its value to that of the electric field, i.e., its steady-state value. Thus, the adiabatic approximation is valid. If this is not the case, the transient part will evolve in a slower time scale than the steady-state part (which is driven by a short duration force, the electric field), increasing the duration of the pulse and even inducing the formation and amplification of a wake [9,23,34]. It is worth mentioning that, while not obvious, Eq. (8) tends to Eq. (9) when $\sigma \gg \gamma^{-1}$ [or, conversely, $\frac{P_{\rm NA}(t_{\rm max}^{\rm NA})}{P_{\rm ad}(t_{\rm max}^{\rm ad})} \to 1$; see Eq. (11)]. This is easily shown by plotting both equations for greater and greater σ or γ.

In conclusion, the adiabatic approximation not only overestimates the maximum value of the polarization but also underestimates its temporal duration. Equation (11) serves as an estimation of how good is the adiabatic approximation. For example, for $\gamma = 8.3 \times 10^{11}$ s^{-1} and an UV seed pulse of 1.5 ps of FWHM ($\sigma = 901$ fs), which are typical values in nitrogen lasing experiments [9,14], $\frac{P_{\rm NA}(t_{\rm max}^{\rm NA})}{P_{\rm ad}(t_{\rm max}^{\rm ad})} = 0.71$ and the adiabatic approximation is not valid. However, if the dipole dephasing rate is increased one order of magnitude while maintaining the duration of the pulse, Eq. (11) gives a ratio of $\frac{P_{\rm NA}(t_{\rm max}^{\rm NA})}{P_{\rm ad}(t_{\rm max}^{\rm ad})} = 0.99$, and thus the adiabatic approximation is valid. The same result is obtained when, instead of the dipole dephasing rate, the duration of the pulse is increased one order of magnitude.

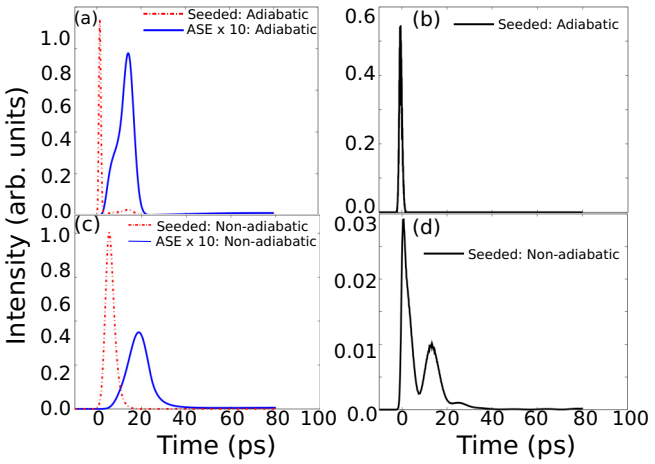

FIG. 4. Comparison of the adiabatic (upper panel) and nonadiabatic (lower panel) polarization for the (a), (c) forward and (b), (d) backward cases. (a) and (c) depict in the red dotted line the forward amplified seed and in the blue continuous line the ASE. The adiabatic approximation cannot explain the temporal profiles of the amplified pulses, with the disagreement in the backward case being more dramatic.

Figure 4 compares the results of using adiabatic and nonadiabatic polarization, both using the time-dependent electron-neutral dephasing rate described in Sec. III. As expected, the adiabatic approximation cannot explain the delay of the peak (4.5 ps experimentally, 5.4 ps nonadiabatic model, 1.3 ps

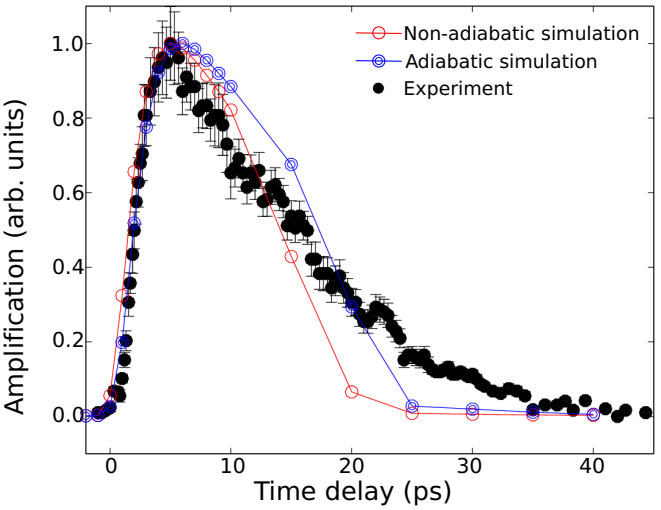

FIG. 5. Experimental amplification curve (black dots) and modeled amplification curves using the adiabatic approximation (blue concentric circles) and the nonadiabatic polarization (red circles).

adiabatic model) and the pulse duration (3.3 ps experimentally, 4.5 ps nonadiabatic model, 1.1 ps adiabatic model) and overestimates the intensity of the ASE. The disagreement between experiment and the adiabatic model is more dramatic in the backward case, where the adiabatic approximation does not develop the longstanding wake observed experimentally.

Figure 5 shows the experimental amplification curve [9] and its modelization with the nonadiabatic model and the adiabatic approximation. The quantity measured is the total emitted energy. Since the gain evolves on a scale of tens of picoseconds, the energy, for an unsaturated amplifier as in this case, depends only on the population inversion and not on the temporal profile of the pulse (provided it is shorter than the characteristic time of evolution of the gain). For this reason, both models explain the curve quite well.

V. CONCLUSIONS

In conclusion, Maxwell-Bloch modeling combined with recent pump-seed experiments have allowed us to unveil the nonadiabatic nature of the amplification of UV radiation in free-space molecular nitrogen amplifiers. Moreover, the temporal profile of amplified UV pulses demonstrates that electron-neutral collisions dominate the dipole dephasing rate, thus probing the temporal variation of electron density and temperature in the plasma along hundreds of picoseconds. This nonadiabatic behavior, along with the strong influence of the temporal evolution of electron-neutral collisions, is of great importance for backward lasing emission, since it sweeps the whole gain dynamics of the plasma during backward propagation. The range of application of the radiative transfer equation (i.e., the adiabatic approximation) has been stated. It is expected that the application of the full Maxwell-Bloch formalism to free-space lasing of N_2 and N_2^+ in air will prove fruitful in the quest for atmospheric backward lasing.

Finally, it is worth mentioning that plasma hydrodynamics may play a role mainly in backward amplification. While most forward amplification takes place some tens of picoseconds after the IR pulse (and thus no hydrodynamic effects are expected), backward geometry implies that the wake of the amplified pulse (which lasts several tens of picoseconds) arrives at the opposite end of the plasma, $z = L$, at a time $t = L/c$ after the IR pulse (for example, for a 3-cm plasma such as the one described in this paper, the head of the backward amplified pulse arrives 100 ps after the IR pulse). Plasma hydrodynamics might affect the amplification by further lowering the electron density. This reduction in density, and its consequent reduction of the collisional dipole dephasing rate, could explain the longer and weaker pulse observed experimentally [Fig. 3(d)] compared with the one given by our model [Fig. 3(b)]. In addition to this, radial gradients of electron density, induced by hydrodynamic expansion or by the spatial profile of the IR pulse, may also impact the one-dimensional (1D) results shown in this paper. For this reason, the three-dimensional (3D) time-dependent Maxwell-Bloch code DAGON [35], an evolution of DEEPONE, will be used in the future to study the impact of electron density inhomogeneities and temporal evolution. The impact of taking advantage of picosecond filamentation in air [36] will also be left for future studies.

ACKNOWLEDGMENTS

The authors acknowledge useful discussions with M. Cotelo, A. González, P. Martínez, J. Moreno, E. Vázquez, P. Velarde, and P. Zeitoun. E.O. acknowledges the support from Spanish Ministerio de Educación, Cultura y Deporte through the Plan Nacional research program, Grant No. ENE2012-32108, the People Programme (Marie Curie Actions) of the European Union's Seventh Framework Programme (FP7/2007-2013) under REA Grant Agreement No. 627191, project DAGON, and the European Union's Horizon 2020 research and innovation programme under Grant Agreement No. 665207 VOXEL. The work is supported in part by the National Natural Science Foundation of China (Grant No. 11574213), Y.L. acknowledges the support by The Program for Professor of Special Appointment (Eastern Scholar) at Shanghai Institutions of Higher Learning (Grant No. TP2014046).

[1] V. Kocharovsky, S. Cameron, K. Lehmann, R. Lucht, R. Miles, Y. Rostovtsev, W. Warren, G. R. Welch, and M. O. Scully, Proc. Natl. Acad. Sci. USA **102**, 7806 (2005).

[2] A. Dogariu, J. B. Michael, M. O. Scully, and R. B. Miles, Science **331**, 442 (2011).

[3] P. Sprangle, J. Peñano, B. Hafizi, D. Gordon, and M. Scully, Appl. Phys. Lett. **98**, 211102 (2011).

[4] A. J. Traverso, R. Sanchez-Gonzalez, L. Yuan, K. Wang, D. V. Voronine, A. M. Zheltikov, Y. Rostovtsev, V. A. Sautenkov, A. V. Sokolov, S. W. North, and M. O. Scully, Proc. Natl. Acad. Sci. USA **109**, 15185 (2012).

[5] P. R. Hemmer, R. B. Miles, P. Polynkin, T. Siebert, A. V. Sokolov, P. Sprangle, and M. O. Scully, Proc. Natl. Acad. Sci. USA **108**, 3130 (2011).

[6] D. Kartashov, S. Ališauskas, G. Andriukaitis, A. Pugžlys, M. Shneider, A. Zheltikov, S. L. Chin, and A. Baltuška, Phys. Rev. A **86**, 033831 (2012).

[7] J. Peñano, P. Sprangle, B. Hafizi, D. Gordon, R. Fernsler, and M. Scully, J. Appl. Phys. **111**, 033105 (2012).

[8] A. Laurain, M. Scheller, and P. Polynkin, Phys. Rev. Lett. **113**, 253901 (2014).

[9] P. Ding, E. Oliva, A. Houard, A. Mysyrowicz, and Y. Liu, Phys. Rev. A **94**, 043824 (2016).

[10] P. N. Malevich, R. Maurer, D. Kartashov, S. Ališauskas, A. A. Lanin, A. M. Zheltikov, M. Marangoni, G. Cerullo, A. Baltuška, and A. Pugžlys, Opt. Lett. **40**, 2469 (2015).

[11] S. Mitryukovskiy, Y. Liu, P. Ding, A. Houard, and A. Mysyrowicz, Opt. Express **22**, 12750 (2014).

[12] P. Ding, S. Mitryukovskiy, A. Houard, E. Oliva, A. Couairon, A. Mysyrowicz, and Y. Liu, Opt. Express **22**, 29964 (2014).

[13] J. Yao, H. Xie, B. Zeng, W. Chu, G. Li, J. Ni, H. Zhang, C. Jing, C. Zhang, H. Xu, Y. Cheng, and Z. Xu, Opt. Express **22**, 19005 (2014).

[14] D. Kartashov, S. Ališauskas, A. Pugžlys, M. Shneider, and A. Baltuška, J. Phys. B: At., Mol. Opt. Phys. **48**, 094016 (2015).
[15] B. Ecker, E. Oliva, B. Aurand, D. C. Hochhaus, P. Neumayer, H. Zhao, B. Zielbauer, K. Cassou, S. Daboussi, O. Guilbaud, S. Kazamias, T. T. T. Le, D. Ros, P. Zeitoun, and T. Kuehl, Opt. Express **20**, 25391 (2012).
[16] Y. Wang, S. Wang, E. Oliva, L. Li, M. Berrill, L. Yin, J. Nejdl, B. M. Luther, C. Proux, T. Le, J. Dunn, D. Ros, P. Zeitoun, and J. J. Rocca, Nat. Photonics **8**, 381 (2014).
[17] G. Li, C. Jing, B. Zeng, H. Xie, J. Yao, W. Chu, J. Ni, H. Zhang, H. Xu, Y. Cheng, and Z. Xu, Phys. Rev. A **89**, 033833 (2014).
[18] P. Wang, C. Wu, M. Lei, B. Dai, H. Yang, H. Jiang, and Q. Gong, Phys. Rev. A **92**, 063412 (2015).
[19] Z. Li, W. Chu, B. Zeng, J. Yao, G. Li, H. Xie, Z. Wang, and Y. Cheng, J. Phys. B: At., Mol. Opt. Phys. **49**, 065602 (2016).
[20] J. Yao, G. Li, C. Jing, B. Zeng, W. Chu, J. Ni, H. Zhang, H. Xie, C. Zhang, H. Li, H. Xu, S. L. Chin, Y. Cheng, and Z. Xu, New J. Phys. **15**, 023046 (2013).
[21] H. Xie, G. Li, W. Chu, B. Zeng, J. Yao, C. Jing, Z. Li, and Y. Cheng, New J. Phys. **17**, 073009 (2015).
[22] D. Kartashov and M. N. Shneider, J. Appl. Phys. **121**, 113303 (2017).
[23] E. Oliva, P. Zeitoun, M. Fajardo, G. Lambert, D. Ros, S. Sebban, and P. Velarde, Phys. Rev. A **84**, 013811 (2011).
[24] O. Larroche, D. Ros, A. Klisnick, A. Sureau, C. Möller, and H. Guennou, Phys. Rev. A **62**, 043815 (2000).
[25] S. Chandrasekhar, Rev. Mod. Phys. **15**, 1 (1943).
[26] T. Tabata, T. Shirai, M. Sataka, and H. Kubo, At. Data Nucl. Data Tables **92**, 375 (2006).
[27] S. Mitryukovskiy, Y. Liu, P. Ding, A. Houard, A. Couairon, and A. Mysyrowicz, Phys. Rev. Lett. **114**, 063003 (2015).
[28] Y. B. Zel'dovich and Y. P. Raizer, *Physics of Shock Waves and High-Temperature Hydrodynamic Phenomena* (Dover, New York, 2002).
[29] V. F. Papakin and A. Y. Sonin, Sov J Quantum Electron **15**, 581 (1985).
[30] J. Yao, B. Zeng, H. Xu, G. Li, W. Chu, J. Ni, H. Zhang, S. L. Chin, Y. Cheng, and Z. Xu, Phys. Rev. A **84**, 051802 (2011).
[31] C. Jing, J. Yao, Z. Li, J. Ni, B. Zeng, W. Chu, G. Li, H. Xie, and Y. Cheng, J. Phys. B: At., Mol. Opt. Phys. **48**, 094001 (2015).
[32] A. Yariv, *Quantum Electronics* (Wiley, New York, 1988).
[33] A. Sureau and P. B. Holden, Phys. Rev. A **52**, 3110 (1995).
[34] I. R. Al'miev, O. Larroche, D. Benredjem, J. Dubau, S. Kazamias, C. Möller, and A. Klisnick, Phys. Rev. Lett. **99**, 123902 (2007).
[35] E. Oliva, M. Cotelo, J. C. Escudero, A. González-Fernández, A. Sanchís, J. Vera, S. Vicéns, and P. Velarde, Proc. SPIE **10243**, 1024303 (2017).
[36] A. Schmitt-Sody, H. G. Kurz, L. Bergé, S. Skupin, and P. Polynkin, New J. Phys. **18**, 093005 (2016).